Density and mineralogy variations as a function of porosity in Miocene Monterey Formation oil and gas reservoirs in California

Caren Chaika and Loretta Ann Williams

ABSTRACT

The Miocene Monterey Formation, long known as the critical source rock in California, also includes significant fractured chert and porous diatomite reservoirs. What is not widely recognized is that there are high matrix porosity reservoirs within the opal-CT and quartz-phase rocks. Using density, porosity, and mineralogy data, we have identified two distinct groups of Monterey Formation reservoirs. group 1 porosity changes gradually during silica diagenesis—porosities of 55–70% exist not only in opal-A–dominated samples but also in samples that have undergone the transition from opal-A to opal-CT. In group 2, porosity decreases abruptly at the transition, and rocks below the transition are tight.

The main mineralogic difference between groups 1 and 2 is a higher clay content in group 1, resulting in different silica diagenesis pathways for the two groups. This led us to expect all San Joaquin basin samples to fall into group 1, and all coastal California samples to fall into group 2, because of the different depositional histories of the two areas. Although our prediction holds in most instances, we discovered that some San Joaquin basin samples exhibit group 2 characteristics. Therefore, it is important to use petrophysical, seismic, and/or geological information to determine if a Monterey Formation reservoir is likely to be a fracture-dominated type (group 2) or if there might be a matrix production component (group 1).

Once one has made this diagnosis, the characteristic density/porosity relationships of each group allow one to easily calculate an accurate matrix porosity.

INTRODUCTION

The Monterey Formation has long been known as the critical hydrocarbon source rock in California. Many petroleum geologists

Manuscript received October 28, 1999; revised manuscript received February 16, 2000; final acceptance March 21, 2000.

AUTHORS

CAREN CHAIKA ~ *Department of Geological and Environmental Sciences, Stanford University, Stanford, California, 94305–2115; current address: Occidental of Elk Hills, Inc., P. O. Box 1001, Tupman, California, 93276-1001; caren_chaika@oxy.com*

Caren Chaika received her B.A. degree in geology from Rice University in 1993 and her Ph.D. from Stanford University in 1998, where she combined geology and rock physics to better understand physical property changes during silica diagenesis. She has been a summer geologist for the Naval Research Laboratory at Stennis Space Center, Mississippi, and for the U.S. Geological Survey in Menlo Park, California. She is currently a production geologist with Occidental of Elk Hills, located near Bakersfield, California.

LORETTA ANN WILLIAMS ~ *Independent Consultant, 2354 Moline Street, Aurora, Colorado, 80010; lorettaann53@hotmail.com*

Loretta Ann Williams has specialized in fine-grained carbonate and silica source rocks that serve as reservoirs. A past Sproule Award recipient, she holds a B.S. degree from SUNY–Stony Brook, an M.B.A. degree from University of Denver, and a Ph.D. from Princeton University. She served as a Stanford University postdoctoral research affiliate from 1981 to 1983 and as an exploration geologist for Champlin Petroleum from 1984 to 1986. Her career has spanned exploration, production, and remediation consulting. She is with PARSEC Group in Denver, Colorado.

ACKNOWLEDGEMENTS

We appreciate the time and effort that Jim Rogers and Mark Longman have put into preparing this volume. We thank Mobil for core from South Belridge field and Chevron for cores from Cymric, Asphalto, and McKittrick fields and for funding for mineralogic analysis. The California State University at Bakersfield Core Repository provided a Shell core from North Belridge field, and we are grateful to this valuable facility, which would not have existed without the efforts of the late Vic Church. Loretta Ann Williams dedicates her work in this article to his memory. Caren Chaika expresses her gratitude to the Stanford Rock Physics Project for use of laboratory facilities, funding, and equipment training, and she appreciates the guidance of Jack Dvorkin, J. G. Liou, and Stephan Graham in her thesis project. We also thank Tony Reid and Jana McIntyre of Occidental Petroleum for allowing us access to their data for Elk Hills field. We are grateful for the work of John Compton and Caroline Isaacs, which supplied our coastal California data. Finally, we are thankful for the work of the numerous investigators who have studied the Monterey Formation, California tectonics, and oceanic upwelling systems before us. Without the body of knowledge their work has provided, this article would not have been possible. This work was supported by the Petroleum Research Fund of the American Chemical Society Grant ACS-PRF #32743-AC2.

now also regard it as one of the last reservoir frontiers in the state. The focus of production to date has largely been on coastal California fractured cherts that have no matrix porosity and on the high matrix porosity diatomites in which silica is in the form of billions of opaline microfossils. We are beginning to realize, however, that in some oil-producing areas of California, Monterey Formation reservoirs produce from high matrix porosity in rocks that have undergone diagenetic transformation from the microfossil opal-A to the intermediate, denser phase opal-CT and even some that have undergone final transition to the stable, dense quartz phase. This discovery has important implications for understanding the unit's true reservoir potential.

Monterey Formation silica originated as biochemically precipitated siliceous skeletal elements, such as sponge spicules, radiolarian tests, and diatom frustules—that is, as amorphous silica colloids (Hurd, 1983). In the sediments, this opaline silica undergoes diagenetic change over time to the stable silica polymorph, quartz, through the pathway opal-A → opal-CT → quartz (Murata and Larsen, 1975; Oehler, 1975; Isaacs, 1980; Williams et al., 1985; and many others).

In deep-sea biogenic siliceous oozes, transitions have such a marked impact on rock properties that they sometimes create strong acoustic reflectors (McManus et al., 1970; Wise and Weaver, 1974; Hein et al., 1978; Bohrmann et al., 1992). Such reflectors sometimes occur in the Monterey Formation at the opal-A/opal-CT or the opal-CT/quartz boundary (Gayle Ehret, 1984, personal communication; Mayerson and Crouch, 1994; Mayerson et al., 1995; Rob Sterling, 1998, personal communication) and signal important changes in petrophysical properties (Isaacs, 1981) that tie directly into reservoir behavior and sound reservoir production practices. A typical diatomite reservoir exhibits porosity of 55–70%, permeability of less than 10 md, and poor induration leading to poor rock competence. After undergoing diagenesis to opal-CT, porosity typically drops from around 45 to below 25%, permeability drops to negligible levels, and the rock becomes well-indurated and brittle. At the transition to quartz, porosity decreases to 0–20%, and the rock becomes even more brittle. Thus, opal-A reservoirs are matrix porosity–dominated reservoirs. Opal-CT and quartz reservoirs, although sometimes maintaining some matrix porosity, are commonly fracture dominated. As with almost every generalization one can make about the enigmatic Monterey Formation, however, there are exceptions to this rule. The giant Elk Hills field, for example, has significant production from fine-grained Monterey Formation biogenic silica reservoirs. As discussed by Reid and McIntyre (2001), extensive coring and analysis indicate that much of the production is from matrix porosity–dominated quartz reservoirs. Further, although a clearly defined opal-A/opal-CT boundary reflector occurs in some locales, there are many Monterey Formation–containing parts of California where there is no reflector.

In this article, we examine matrix porosity preservation in Monterey Formation reservoirs, associated petrophysical properties, and

physical and chemical reasons for porosity preservation beyond the opal-A diagenetic stage.

GEOGRAPHIC AND DEPOSITIONAL SETTING

The Monterey Formation is a Miocene biogenic siliceous deposit that underlies much of southern California (Figure 1), achieving thicknesses greater than 2000 ft (610 m) in some places. It is an important petroleum source and reservoir rock in two general areas: (1) coastal California from Monterey south to near San Diego, and (2) the San Joaquin Valley. Many of California's largest oil fields produce in part from fine-grained Monterey Formation reservoirs—for example, the Ventura basin Oxnard field and the San Joaquin basin Cymric field, which have so far produced 12 million and 19 million bbl of oil, respectively, from the Monterey Formation (CDOC, 1998). Cook (1994) estimated a statewide total of 10 billion bbl of oil in place remaining in Monterey Formation siliceous reservoirs.

In general, Monterey Formation style deposition occurred owing to a unique Miocene combination of climatic, oceanographic, and tectonic conditions (Ingle, 1981; Pisciotto and Garrison, 1981; Isaacs, 1983; Luyendyk and Hornafius, 1987; Schoell et al., 1994). Many investigators have studied the formation's depositional and diagenetic origin (e.g., Bramlette, 1946; Isaacs, 1980; Blake, 1981; Graham and Williams, 1985; and many others). To summarize, California was tectonically active in the Miocene, primarily due to San Andreas transform fault movement. Wrench tectonics created silled, restricted ocean basins in the areas that now contain Monterey Formation deposits. High rates of coastal upwelling of nutrient-rich waters led to high biologic productivity in these basins, including planktonic diatom blooms. Organic debris falling through the water column was oxidized, causing waters below wave base to become oxygen depleted. Restricted water circulation due to the silled sea bottom topography contributed to this development of low oxygen bottom waters that are so important to preserving organic matter in sediments. Although very fine-grained, like most biogenic siliceous deposits throughout time, there is a great deal of subtle variation in Monterey Formation lithologies—commonly on a bed-to-bed scale—that directly impacts source and reservoir quality. This is due to a combination of original depositional components and fabrics and diagenetic history.

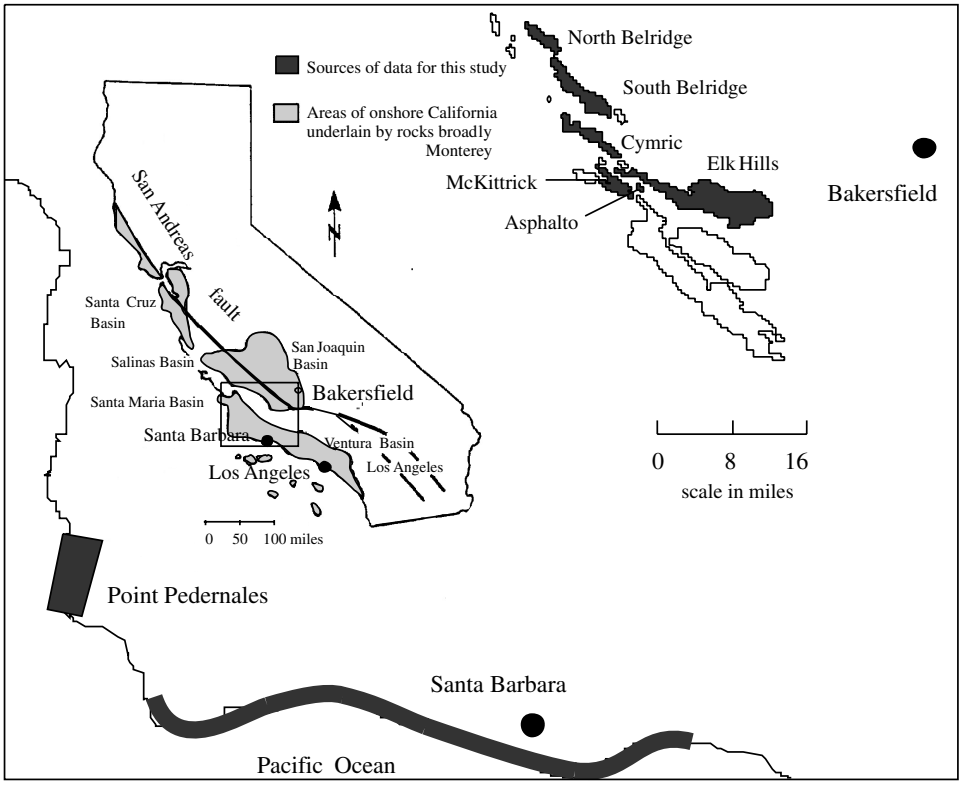

Figure 1. Geographic extent of Monterey Formation and Monterey-type Miocene deposits of onshore California, and specific sample areas for this study. Original analyses for this article come from cores in Asphalto, North and South Belridge, Cymric, and McKittrick oil fields and are supplemented by core data from Elk Hills field collected by Reid and McIntyre (2001) and outcrop data collected by Compton (1991) at Point Pedernales and Isaacs (1980) along the Santa Barbara coast.

Coastal California Monterey Formation siliceous rocks are generally cleaner (contain fewer clastics) than the dirty San Joaquin Valley Monterey Formation biogenic siliceous rocks. The San Joaquin Valley was an inboard basin in the Miocene, receiving clastic input from the Sierra Nevada Mountains on the east and the emergent Salinian Block to the west. The coastal basins were outboard basins, isolated from mainland clastics by the Salinian Block and other sills. The resulting difference in detrital influx resulted in two distinctly different Monterey Formation reservoir styles. We have chosen our sample database to reflect both.

METHODS

Our study is based on dry bulk density ($\rho_{b(dry)}$), grain density (ρ_s), and porosity (ϕ) measurements, along with mineralogic analyses for cores from five fields in the San Joaquin Valley (Asphalto, Cymric, McKittrick, North Belridge, and South Belridge) and outcrop samples from Point Pedernales and the Santa Barbara area (Figure 1). San Joaquin data are a combination of original data and data collected by Core Laboratories (Appendix). The coastal California data are from published information of Compton (1991) and Isaacs (1980). Our efforts to minimize unsystematic error arising from measurements in different laboratories and/or using different methods are presented in the Appendix, along with a table of all unpublished data used in this article. Most important, Isaacs's (1980) methodology for measuring porosity was very different from that used in collecting the other data. We therefore only use her data in our mineralogic evaluations, where density and porosity are not considered.

We selected only samples having biogenic silica $\geq$ 40 wt. %. Based on the classification scheme of Williams (1982), this cutoff includes the following lithologies: diatomite (>80 wt. % opal-A), diatomaceous shale (40–80 wt. % opal-A), chert (>80 wt. % opal-CT and/or quartz), porcelanite (50–80 wt. % opal-CT and/or quartz), and the higher end of the siliceous shale range (20–50 wt. % opal-CT and/or quartz). It eliminates clastic-dominated and carbonate-dominated lithologies.

Our analysis of density and porosity behavior of Monterey Formation rocks relies on the basic relationship (e.g., Schlumberger, 1989)

$$\rho_{b(sat)} = \rho_s(1 - \phi) + \rho_f\phi \quad (1)$$

where $\rho_{b(sat)}$ = saturated density of the rock, expressed as total weight/total volume; ρ_s = total weight of rock solids/total volume of rock solids; and ρ_f = total weight of fluids in the rock/total volume of fluids in the rock. Because analyses used in this study are from dried cores, $\rho_f = 0$, and the equation simplifies to

$$\rho_{b(dry)} = \rho_s(1 - \phi) \quad (2)$$

where $\rho_{b(dry)}$ = total dry weight/total dry volume.

For comparison, we used the standard quartz density of 2.654 g/cm^3 (Schlumberger, 1989). Opal-CT, not a true mineral, varies widely in density. We used the density of a nonporous hydrothermal tridymite sample as our approximation of the ideal opal-CT (Appendix).

PATTERNS OF POROSITY REDUCTION

Silica phase transitions cause changes not only in porosity but in density as well. In the Monterey Formation (Isaacs, 1981; Compton, 1991), $\rho_{b(dry)}$ ranges from 0.7–1.2 g/cm^3 for opal-A rocks, to 1.1–2.0 g/cm^3 for opal-CT rocks, to 1.9–2.6 g/cm^3 for quartz rocks. This information, coupled with the associated porosity changes mentioned previously, suggests a distinctive porosity/density pattern should emerge as a rock sequence undergoes diagenesis. To examine this relationship, we plotted $\rho_{b(dry)}$ against ϕ (Figure 2). Because ϕ was directly measured, whereas $\rho_{b(dry)}$ was for the most part calculated (Appendix), $\rho_{b(dry)}$ was the requisite dependent variable. The result was two distinct linear relationships:

$$\rho_{b(dry)} = 2.50 - 2.60\phi;\ R^2 = 0.990;\ n = 39 \quad (3)$$

and

$$\rho_{b(dry)} = 2.13 - 2.07\phi;\ R^2 = 0.936;\ n = 33 \quad (4)$$

where R^2 = correlation coefficient, and n = number of samples upon which the regression is based.

Equation 3 characterizes the Belridge, Cymric, and Asphalto core samples, and equation 4 characterizes the McKittrick core and Point Pedernales outcrop samples. The lines intersect at $\phi = 0.70$, meaning that these high porosity rocks have the same dry bulk den-

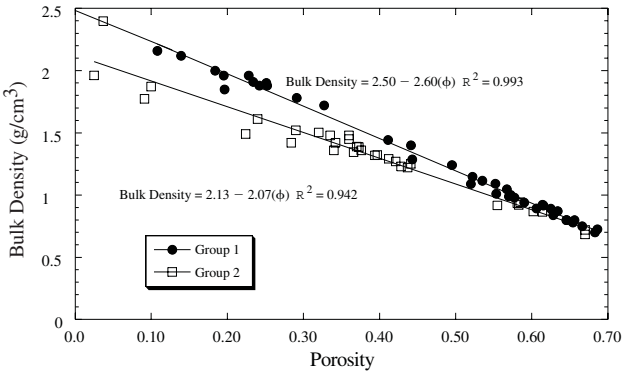

Figure 2. Dry bulk density vs. porosity plot for core data from Asphalto, North and South Belridge, Cymric, and McKittrick oil fields (Appendix) and Point Pedernales outcrop data of Compton (1991). All oilfield data except those for McKittrick field fall on the group 1 line. McKittrick field core data and Point Pedernales outcrop data fall on the group 2 line, except for a Point Pedernales quartz chert (open square), which has a higher density than the other opal-A and opal-CT Point Pedernales samples.

sity regardless of which regression trend they follow. Indeed, the lines are practically indistinguishable for all ϕ greater than about 55% (predominantly diatomaceous rocks). Rocks lying on the equation 3 line that have ϕ less than 55% have higher densities than rocks lying on the equation 4 line. The higher negative slope of equation 3 indicates a greater rate of density change with porosity reduction than for equation 4 samples. If $\rho_{b(dry)}$ is a function of silica phase, this result suggests that equation 3 reflects either a more rapid rate of phase transition or a longer porosity retention relative to equation 4.

The high R^2 value for both lines indicates that ϕ changes are almost wholly sufficient to explain $\rho_{b(dry)}$ changes. Because the trends are so strong, we hereafter distinguish them as group 1 (rocks having ϕ/ρ_b characteristics described by equation 3) and group 2 (rocks having ϕ/ρ_b characteristics described by equation 4). For each group, one can predict $\rho_{b(dry)}$ with a high degree of certainty if one knows ϕ. It is more useful to be able to predict ϕ from $\rho_{b(dry)}$. Therefore, as discussed in a following section, we develop a method for porosity estimation from either dry bulk densities measured directly from core or wire-line density log readings of saturated bulk density.

Note that one group 2 point plots directly on the group 1 line, at $\phi = 0.037$, $\rho_{b(dry)} = 2.40$. This sample, the only quartz data point from the Point Pedernales outcrop, illustrates an important point. Projecting equation 4 out to $\rho_{b(dry)} = 2.65$ g/cm^3 yields a porosity of −28%, which is impossible. In reality, equation 4 ends in a steep curve that must have an inflection point in the range of $\phi = 0$–10% porosity, as rocks of increasing density converge on 0% porosity.

For the relationship of $\rho_{b(dry)}$ to ρ_s in equation 2 to be linear, ρ_s must be a constant that describes the regression line slope, an assumption critical to the standard density method of estimating porosity from logs (Tom Zalan, 1997, personal communication). In this situation, a density of zero must yield 100% porosity—that is, where there are no grains to create density, the rock is 100% pore space. Neither equation 3 nor equation 4, however, passes through the $\phi = 1$, $\rho_{b(dry)} = 0$ point (Figure 3), indicating that solid phase density changes with porosity reduction. We know from previous authors' work that silica phase density changes as porosity decreases. The fact that our data support this trend, having a strong R^2, indicates that silica phase change is a dominating factor in porosity decrease in these rocks.

Our next logical step is to plot ρ_s vs. ϕ, resulting in two distinct nonlinear plots:

$$\text{Group 1: } \rho_s = 2.52 + 0.27\phi - 0.96\phi^2; \quad R^2 = 0.737 \tag{5}$$

and

$$\text{Group 2: } \rho_s = 1.92 + 1.42\phi - 1.61\phi^2; \quad R^2 = 0.492 \tag{6}$$

This confirms that grain density changes as porosity decreases, as one would expect if silica phase changes are affecting the trends (Figure 3). We have eliminated the aberrant quartz chert point in group 2 that plots on the group 1 line, because it falls within the nonlinear part of group 2, which is outside of the scope of this study.

Porosity explains 74% of the grain density trend for group 1 rocks but only 49% of the grain density trend for group 2 rocks. Thus, although there is a very strong relationship between porosity and bulk density, porosity is not as useful in explaining grain density relationships. This is because different minerals have different grain densities, but a rock made up of different minerals can still have the same porosity. For example, for a pure quartz sandstone, ρ_s is close to 2.65 g/cm^3, whereas for a pure dolomite, ρ_s is close to 2.85 g/cm^3 (e.g., Schlumberger, 1989), but both rocks may have 30% porosity. In the context of this data set, the fact

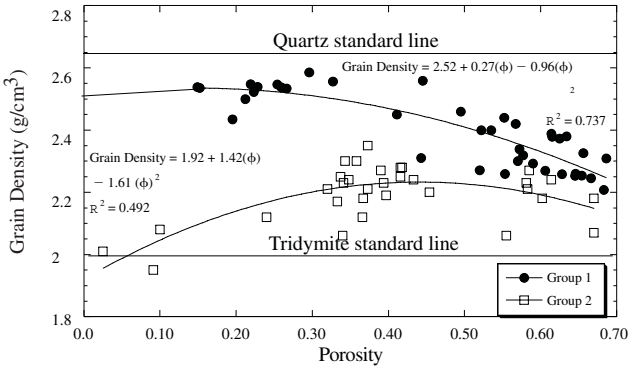

Figure 3. Grain density vs. porosity plot for the data of Figure 2. Ideal quartz grain density is assumed to be 2.654 g/cm^3 (Schlumberger, 1989), regardless of sample porosity. Ideal opal-CT density is assumed to lie somewhere around the grain density of pure tridymite as determined in our study (Appendix), regardless of sample porosity.

that groups 1 and 2 separate so distinctly in solid density indicates that they must be compositionally different. The low R^2 characteristic of each group, however, evidences a high degree of intragroup variability—particularly for group 2 rocks.

With decreasing ϕ, group 1 ρ_s generally increases toward the density of the mineral quartz, whereas group 2 ρ_s remains low and even decreases toward the average density of the disordered mineraloid opal-CT. It appears that group 1 rocks must undergo diagenesis all the way to quartz before losing most of their porosity, whereas group 2 rocks lose most of their porosity in the opal-CT conversion. This is due to either a more rapid phase transition rate or slower rate of porosity decrease in group 1.

At high porosity, opal-A is the dominant biogenic silica phase for both groups. Opal-A and opal-CT coexist in group 1 rocks (Figure 4a) at midrange porosities, with opal-CT becoming increasingly dominant. At lower porosities (30% and less), quartz becomes the dominant polymorph. Group 2 rocks (Figure 4b) contain only opal-A at high porosities, which is abruptly replaced with opal-CT at around 45% porosity. Very little quartz (biogenic or detrital) is in any of these group 2 rocks. At low porosities, the rocks are almost totally made up of opal-CT. Thus, one of the distinguishing characteristics of the two groups is that group 1 rocks retain porosity longer during silica diagenesis than do group 2 rocks. Using Isaacs's (1980) data, which includes many group 2 quartz rocks, we confirm the group 2 characteristics (Figure 4c).

If silica diagenetic phase fully explained group 1 and group 2 distinctions, both Figure 3 curves would overlap in the high porosity, low density opal-A and opal-CT range and would only diverge below 40% porosity, where group 1 rocks are entering the quartz phase and group 2 rocks remain in the opal-CT range. Instead, group 1 densities are consistently higher than group 2 densities, regardless of porosity and silica polymorph. Group 1 rocks become increasingly dense as they get tighter, whereas group 2 rocks become less dense as porosity decreases below 40%. Thus, although silica diagenesis impacts ϕ/ρ_b trends, it does not explain them. Figure 4 demonstrates that there is a significant nonsilica component in both group 1 and group 2 rocks, ranging from 5 to 55 wt. % of the rock. This nonsilica component is made up largely of clay minerals, zeolites, and feldspars, of both clastic and diagenetic origin.

Although similar in the ratio of biogenic silica to other minerals in the opal-A stage, group 1 and group 2 rocks differentiate with the transition to opal-CT. group 1 rocks, in which opal-A and opal-CT coexist, remain dirty and have a continuous porosity range (Figure 5a). In group 2 rocks, opal-A and opal-CT appear to be mutually exclusive, and opal-CT rocks are significantly cleaner than their opal-A counterparts. An obvious 8% porosity gap exists from about 45 to 53% at the opal-A to opal-CT transition (Figure 5b).

These observations suggest that group 1 rocks undergo a gradual change in rock properties, including porosity, bulk density, grain density, and mineralogy, during diagenesis. No discontinuity in properties exists to produce an acoustic reflector. Group 2 rocks, however, undergo an abrupt conversion of opal-A to opal-CT, and the boundary is characterized by a stepwise change in porosity, bulk density, grain density, and mineralogy, which is likely to produce an acoustic reflector.

Note here that the acoustic reflector we are referring to is a diagenetically induced reflector only. Silica diagenetic reflectors tend to exhibit normal polarity, whereas gas-related reflectors, which can also occur in the Monterey Formation, exhibit inverse polarity (Shipley et al., 1979; Lonsdale, 1990). This is what one would expect, in that diagenetic reflectors result from an abrupt change from less dense to more dense material. A reflector caused by gas results from a lighter phase in porosity overlain by rocks that have a denser phase (water or ice) in the porosity. Lonsdale (1990) noted, however, that purely diagenetic horizons can exhibit inverse polarity if the transition zone is

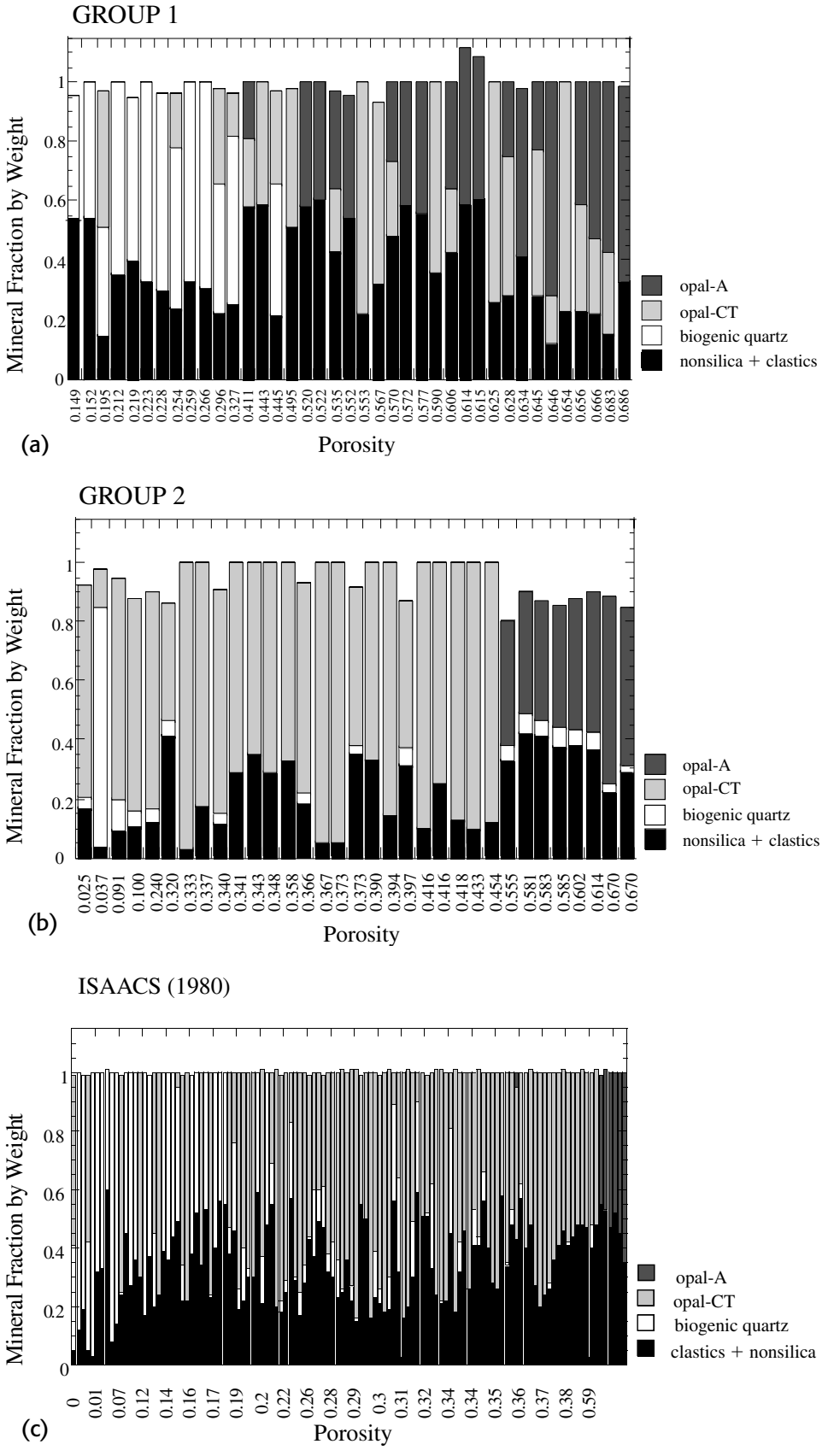

Figure 4. Bar charts of sample percentages by weight of opal-A, opal-CT, biogenic quartz, and nonbiogenic minerals plotted against porosity, in group 1 samples (a), group 2 samples (b), and Isaacs (1980) data (c). Organic carbon and other minor components are not included, measurement methodologies are mixed, and therefore component sums do not always equal 100%. Note that opal-A and opal-CT do not coexist in group 2 samples (b and c). Instead, there is an abrupt transition from opal-A to opal-CT. The two phases do coexist in group 1 samples.

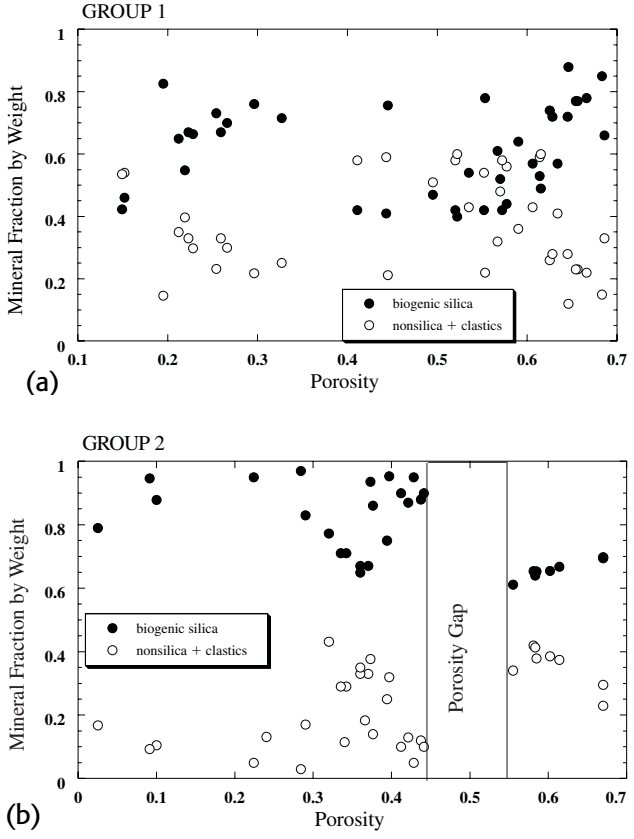

Figure 5. Biogenic silica content vs. other minerals (nonsilica minerals and detrital quartz) as porosity decreases for group 1 (a) and group 2 (b). Note the porosity gap in the group 2 samples, between the opal-A phase at 53% porosity and the opal-CT phases at 45% porosity (b).

complex—the sum of interferences from interbedded opal-A/opal-CT or opal-CT/quartz zones can yield a reverse polarity.

The foregoing analysis has defined two distinctive mineralogical and petrophysical groups, summarized in Table 1. Differences between groups 1 and 2 could be due to stratigraphic, compactional, or geochemical effects, which we discuss in the next sections.

ORIGINS OF GROUP 1 AND GROUP 2 TRENDS

Stratigraphy

A density difference due to relative clay content with porosity reduction may merely signal a stratigraphic change with depth. Generalizing broadly, most diatomaceous rocks in the Monterey Formation and

Table 1. Summary of Distinguishing Petrophysical and Mineralogical Characteristics of Group 1 and Group 2 Monterey Formation Reservoirs

Group 1	Group 2
Lies on group 1 regression line	Lies on group 2 regression line
Continuous porosity range	Porosity gap at 45–53%
Opal-A and opal-CT commonly coexist	Opal-A and opal-CT rarely coexist
No diagenetic reflector likely	Can produce a diagenetic reflector

equivalents are at the stratigraphic top of the formation and were deposited as the basins were filling. As a result, regardless of geographic location, this part of the section tends to be clastic rich. This probably explains why group 1 and group 2 do not show strong density/porosity differentiation in the opal-A range. This is the only time-stratigraphic change likely to affect the data. Below the opal-A diagenetic boundary, stratigraphic members are largely defined based on clastic or carbonate content, and these stratigraphic differences were largely eliminated by our use of only rocks having at least 40 wt. % biogenic silica. Also, the opal-CT and quartz rocks from the five San Joaquin basin cores were taken at different burial depths but in the same general stratigraphic interval, yet the McKittrick field samples plot in group 2, whereas the rest plot in group 1.

Compaction

Mechanical crushing and realignment of grains causes significant volume reduction in any sedimentary rock section during lithification. Visual evidence of mechanical compaction exists in Monterey Formation thin sections, and pressure solution seams known as stylolites are also common (Williams, 1982, 1988). Most workers who have examined porosity reduction in biogenic siliceous rocks have invoked compaction as a primary or secondary mechanism (Iijima and Tada, 1981; Isaacs, 1981; Tada and Iijima, 1983; Compton, 1991).

At first glance, the group 1 ρ_b/ϕ curve (Figure 3) is shaped very much like a typical compaction curve, and this makes sense. As porosity decreases, there are more grains per unit volume of rock and so density should increase. Equation 2, however, by which solid

density is derived, corrects for this porosity variation effect, and therefore the resemblance is an illusion. Also, rocks do not become less dense during compaction, as appears to be happening in group 2. Therefore, compaction, although an important part of the overall picture, is not a likely factor in explaining group 1 and group 2 differences shown in Figure 3.

Although experimental velocity measurements of cores (Chaika, 1998) provided evidence of some compaction effects in opal-A/opal-CT transition rocks, a continuous compaction curve model does not predict the gap in porosity observed in group 2 rocks at the opal-A/opal-CT boundary (Figures 4b and 4c). Recall that in group 2 rocks, opal-A and opal-CT do not coexist (Figure 4b). Isaacs (1981) attributes the lack of phase coexistence, plus the sharp porosity change at the phase boundary, to a sudden compactional event as silica dissolved and changed phase from opal-A to opal-CT. She suggests that these changes happened quickly, causing the rock to lose its framework strength during dissolution, allowing a compactional collapse. Thus, she sees compaction as an effect of chemical diagenesis.

Although mechanical compaction is a factor in porosity reduction, we agree with Isaacs (1981) that the overriding control on porosity reduction with depth in Monterey Formation rocks lies with geochemical effects, as we inferred from our ρ_b/ϕ graphical results.

SILICA DIAGENESIS AND POROSITY REDUCTION

Silica diagenesis follows the Ostwald step rule, which predicts that, given a constant chemical composition, the first solid to precipitate will be the phase of highest entropy (opal-A), followed by intermediate steps (larger, less irregularly shaped opal-A and opal-CT) to the lowest entropy phase (quartz) (Iler, 1973, 1979; Williams and Crerar, 1985; Chang and Yortsos, 1994). Because silica diagenesis occurs through dissolution-reprecipitation, not solid state transformation, higher entropy phases dissolve and lower entropy phases precipitate. Therefore, the specific pathway taken (size/surface area and phase) depends upon silica concentration in solution. Anything affecting pore-water silica concentration will affect the rates and nature of diagenetic reactions (Williams and Crerar, 1985; Williams et al., 1985; Chang and Yortsos, 1994).

Group 1 and Group 2 Diagenetic Pathways

Previous authors have empirically demonstrated that an abundance of detrital clay minerals in the system retards the opal-A/opal-CT transition and enhances the opal-CT/quartz reaction (Murata and Larsen, 1975: Kästner et al., 1977; Isaacs, 1980, 1983). This is most likely due to adsorption of dissolved silica onto clay surfaces at naturally occurring pH values and the tendency of dissolved silica to complex with metal ions in solution and precipitate as diagenetic clays (Hein et al., 1978; Badaut and Risacher, 1983; Williams et al., 1985).

Coexistence of opal-A and opal-CT in group 1 rocks but uncommonly in group 2 rocks is a consequence of the different amounts of clays (both detrital and authigenic) between these two groups. As opal-A dissolves (having materials of highest surface area dissolving first), silica in solution increases. In group 1 rocks this silica is readily taken up by clays and clay authigenesis, which keeps the degree of silica supersaturation (Ω) low. In the relatively detrital-free group 2 rocks, Ω is larger. Reaction rates are generally proportional to Ω (Williams et al., 1985). Therefore, the opal-A transforms to opal-CT more slowly in group 1 rocks than in group 2 rocks, increasing the likelihood that phases will coexist during the transformation. Also, because the crystals grow more slowly in group 1, porosity is retained further into the diagenetic process. In contrast, in group 2 rocks, high Ω causes more rapid opal-A dissolution followed by opal-CT precipitation.

The specifics of this model are best illustrated graphically. Silica diagenesis of group 2 rocks, which are relatively detrital-free, proceeds along the pathway 1 → 2a → 4 of Figure 6a. Little competition for dissolved silica from detrital phases exists, and so Ω, the degree of supersaturation, becomes large enough to be in equilibrium with the nucleation of small, high surface area opal-CT crystals. Because reaction rates are generally proportional to Ω (Williams et al., 1985), aging proceeds rapidly—that is, crystals grow rapidly to well-ordered, large, euhedral opal-CT crystals that interlock to occlude porosity.

For kinetic reasons, low pore-water silica concentrations favor quartz crystal growth relative to higher concentrations (Williams and Crerar, 1985; Williams et al., 1985)—that is, as Ω decreases, quartz aging rate increases. Although the group 2 opal-CT/quartz transition proceeds along path 4a → 6 of Figure 6a, the rate of aging is impeded by elevated pore-water silica con-

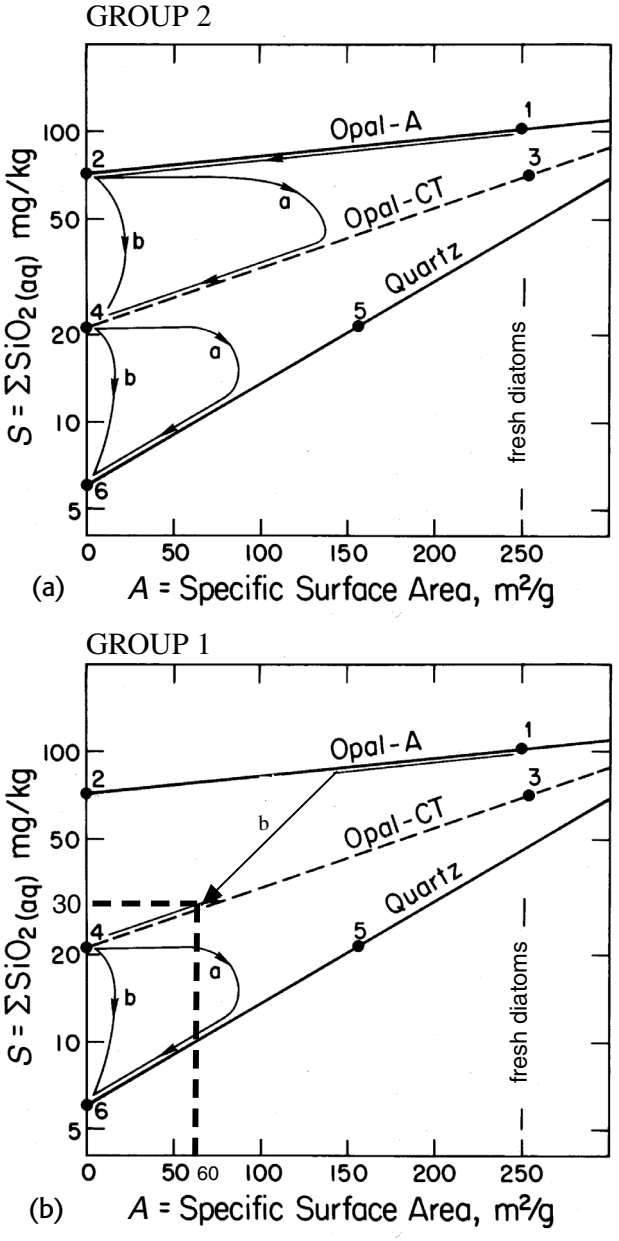

Figure 6. Schematic graph of solubility (*S*) vs. surface area (*A*), showing the silica diagenetic pathway for group 2 rocks (a) and the more clay rich group 1 rocks (b). Note: solubility is plotted on a log scale. Group 2 represents the classic opal-A → opal-CT → quartz pathway. Opal-A diatoms lose surface area through dissolution of frustule ornamentation and fill in frustule pore spaces with coarse-grained, lower surface area precipitates, until surface area decreases to the point that tiny seed crystals of high surface area opal-CT is preferred. This opal-CT ages to lower surface area, larger grained opal-CT, until the solution is saturated only with respect to quartz. At this point, fine seed crystal quartz precipitates and ages to more coarsely crystalline quartz. The group 1 pathway represents the impact of clays on this model. Modified from Williams et al. (1985).

centrations. Therefore, opal-CT persists in group 2 rocks. By the time transition to quartz occurs, the combination of compaction and opal-CT aging has occluded most matrix porosity.

Group 1 rocks follow a different pathway owing to their higher clay content. If we assume that the uptake of dissolved silica by clays depresses Ω to 30 mg/kg as per Williams et al. (1985, p. 308), group 1 samples follow the pathway 1 → 1b → 4 during the opal-A/opal-CT transition (Figure 6b). In this situation, opal-A aging is interrupted at high surface areas, and opal-A diatoms that have diagenetic overgrowths and pore fillings do not occur. Instead, relatively pristine and/or partially dissolved diatoms intermix with opal-CT crystals of 60 m^2/g surface area—large relative to the first opal-CT crystals precipitating in a group 2 sample. At this lower Ω, Ostwald ripening rates (aging to larger, more euhedral crystals) are also slower. Although the first opal-CT crystals to form are larger than those in group 2, they age and grow more slowly. Diagenetic clays occlude some of the porosity, but these clays have high surface areas (which implies irregular shapes), like the opal-CT crystals. Thus, porosity becomes more tortuous, and pore throats are smaller, but porosity persists longer than in group 2 rocks.

At point 4 of Figure 6b, opal-CT surface area/size differences no longer affect solubility, but the solution is still supersaturated with respect to quartz of surface area less than 150 m^2/g, and quartz begins to precipitate, along pathway 4a → 6, just as for group 2. High surface area quartz crystals nucleate, decreasing pore-water silica saturation. This, plus precipitation of clay and zeolites, facilitates quartz precipitation, which proceeds best at low silica concentrations. These ideal silica concentrations for quartz precipitation persist, because as Ω drops too low, clays that adsorbed silica at higher pore-water silica concentrations are out of equilibrium with the new pore-water concentrations and begin to desorb silica. This process buffers pore waters at low silica concentrations where most of the silica in solution is monomeric—the ideal condition for growing quartz crystals and producing epitaxial overgrowths on detrital quartz grains (Williams and Crerar, 1985). Thus, chemical processes keep silica concentration low, which allows quartz transformation at a shallower depth of burial. The group 1 trend toward incomplete porosity occlusion and increasingly tortuous porosity and smaller pore throats continues.

Note here that the effective opal-CT → quartz Ω/surface area pathway is the same (4a → 6 on Figures 6a

and 6b) for groups 1 and 2, but group 1 rocks move more quickly through the opal-CT/quartz transition than group 2 rocks.

Thus, the differences between group 1 and group 2 reservoirs depend largely on the relative amount of detritals and biogenic silica in the rocks. If there is a large amount of clay minerals or potential to form clays, opal-A and opal-CT coexist, there is no porosity gap, and the slow opal-A/opal-CT transition can preserve matrix porosity into the quartz phase. In contrast, if the rock is rich in biogenic silica and poor in detritals, opal-A dissolves rapidly. There is a porosity gap at the opal-A to opal-CT transition, opal-A and opal-CT rarely coexist, and opal-CT and quartz rocks are tight.

The ultimate result of the two pathways of diagenesis are two distinctly different reservoirs. Group 2 reservoirs proceed more rapidly from the high porosity opal-A phase to the opal-CT transition. Group 2 opal-CT and quartz rocks, which have low porosity and low clay content, exhibit the near-homogeneous textures of tightly interlocking crystals that are ideal for competent fracturing behavior under stress (McGill and Raney, 1970). Group 1 rocks retain high porosity opal-A longer and, thus, to a greater burial depth. group 1 opal-CT rocks proceed through the transition to quartz more quickly, at a shallower burial depth and lower compaction level. Having higher clay content, these rocks behave more plastically under stress and so exhibit less large, long, through-going fractures (Grivetti, 1982; Snyder et al., 1983; Williams, 1988; Gross, 1995). Even where unfractured, however, group 1 quartz rocks exhibit reservoir potential owing to oil stored in the 20–40+% matrix porosities.

APPLICATIONS

Statistically speaking, the model we present here is preliminary. It would require much more data to establish the exact group 1 and group 2 regression line equations. Even at this stage, however, the model has several practical applications.

Reservoir Classification

Opal-CT and quartz reservoirs that produce primarily from matrix porosity are just beginning to be recognized in the Monterey Formation, and production practices are beginning to be adapted for the special requirements of such reservoirs. The C/D shale producing unit of Elk Hills field, as described by Reid and McIntyre (2001), appears to be a clear example of a group 1 reservoir. We plotted Elk Hills C/D shale data on the $\rho_{b(dry)}/\phi$ graph of Figure 2 to determine if the quantitative model classifies this reservoir as we expect it should from qualitative characteristics. The model clearly places the C/D shale reservoir in group 1 (Figure 7).

Porosity Prediction from Density Logs

Although rigorous statistical practice required that we use $\rho_{b(dry)}$ as the dependent variable in equations 3 and 4, our 24 measured $\rho_{b(dry)}$ data points were consistent with calculated data within a range of 0.01–0.08 g/cm^3 for 22 out of the 24 samples, having the two outliers at a difference of 0.14–0.15 g/cm^3. We argue that the correspondence is sufficient to allow us to flip the regressions and make ϕ the dependent variable. The result is the following two regression lines:

$$\text{Group 1: } \phi = 0.956 - 0.382\rho_{b(dry)}; \quad R^2 = 0.993;\ n = 39 \tag{7}$$

and

$$\text{Group 2: } \phi = 0.987 - 0.454\rho_{b(dry)}; \quad R^2 = 0.942;\ n = 33 \tag{8}$$

To convert $\rho_{b(dry)}$ to well log bulk density readings, we must resaturate it. Recalling the definition of $\rho_{b(dry)}$

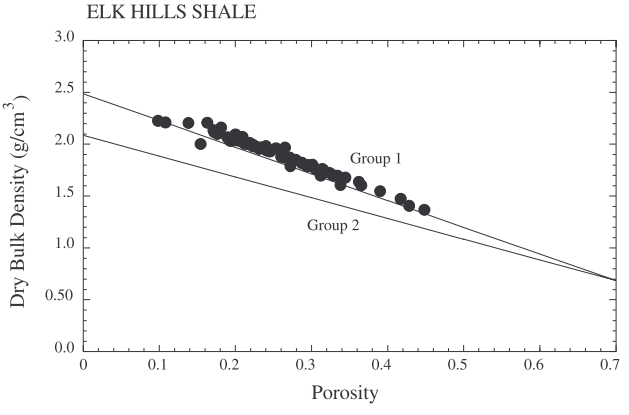

Figure 7. Dry bulk density vs. porosity data for two matrix porosity dominated C/D shale cores from the Elk Hills field plotted against the group 1 and group 2 regression lines of Figure 2. The data are clearly classified as a group 1 reservoir, as expected.

given in equation 2, this resaturation can be expressed as

$$\rho_{b(sat)} = \rho_{b(dry)} + \phi_f \quad (9)$$

Substituting equations 7 and 8 for $\rho_{b(dry)}$ in equation 9 yields

$$\text{Group 1: } \phi = (0.956 - 0.382\rho_{b(sat)}) \div (1 - 0.382\rho_f) \quad (10)$$

and

$$\text{Group 2: } \phi = (0.987 - 0.454\rho_{b(sat)}) \div (1 - 0.454\rho_f) \quad (11)$$

Thus, ϕ can be directly calculated from $\rho_{b(sat)}$ using the group 1 and group 2 relationships. Given an average ρ_f of 0.95 g/cm^3 (Chaika, 1998, p. 74), we can simplify these equations to

$$\text{Group 1: } \phi = 1.501 - 0.600\rho_{b(sat)} \quad (12)$$

and

$$\text{Group 2: } \phi = 1.736 - 0.798\rho_{b(sat)} \quad (13)$$

This gives us a direct relationship between ϕ and $\rho_{b(sat)}$ read from a density log. The $\rho_{b(sat)}$ readings are among the most reliable log information, whereas porosity read directly from the neutron porosity logs is commonly much larger than directly measured helium porosity, because the tool detects water bound in clay minerals and other phases, as well as free fluids in the pores (Schlumberger, 1989). Equations 12 and 13 allow us to circumvent the unreliable neutron porosity log, while replacing the standard density log method of porosity estimation (Schlumberger, 1989) as well. This method assumes that grain density (our ρ_s; Schlumberger's ρ_{ma}) is constant, an assumption that is clearly erroneous for Monterey Formation rocks, whose grain densities range from less than 2.0 to about 2.6 g/cm^3 (Figure 3).

Our method requires only that one assume that the reservoir belong to either group 1 or group 2. It then becomes easy to calculate reservoir matrix porosity reliably from density log information, without having to make an assumption about grain density—even as the well is being drilled! Figure 8 compares neutron porosity, standard density porosity estimation (assumed ρ_s = 2.5 g/cm^3, based on data for group 1 in Figure 3), directly measured porosity, and our calculated porosity for three of the wells used in this study—two from group 1 reservoirs in Cymric and Asphalto fields and one from a group 2 reservoir in McKittrick field.

Neutron porosity tracks measured porosity accurately in the opal-A section of Cymric field but shows poor relationship to true porosity in the opal-CT and quartz reservoirs of Asphalto and McKittrick fields. For the standard density method, Figure 8 points out how critical it is to correctly estimate grain density before calculating porosity. The 2.5 g/cm^3 estimation that we assigned to all three logs works well for the group 1 opal-CT and quartz reservoir of Asphalto field, but greatly overestimates porosity in the group 1 opal-A reservoir of Cymric field and the group 2 opal-CT and quartz reservoir of McKittrick field. Our method estimates porosity well in all three cases.

CONCLUSION

This article indicates that Monterey Formation biogenic siliceous reservoir rocks can be divided into two groups based on petrophysical properties. Porosity, density, and mineralogy data indicate that porosity reduction, although a function of compaction, is even more strongly affected by silica diagenetic conditions. In group 1 rocks, changes in porosity, density, and

Figure 8. Comparisons of neutron porosity logs, standard method density log porosity estimation (grain density assumption of 2.5 g/cm^3), our density method for porosity estimation, and direct porosity measurements on core samples. The neutron porosity log estimates porosity reasonably well in the Cymric opal-A reservoir (c) but overestimates porosity in quartz and opal-CT reservoirs of Asphalto (a) and McKittrick (b) fields. The standard density method works well with our grain density assumption for the group 1 opal-CT and quartz reservoir of Asphalto field (a) but not for the group 2 reservoir of McKittrick field (b) or the group 1 opal-A reservoir of Cymric field (c). In order for this method to work, the grain density assumption would have to be changed for each reservoir. The method developed in this article is a fairly good estimator of porosity for all three reservoir types and requires only that one correctly choose the group to which the reservoir belongs.

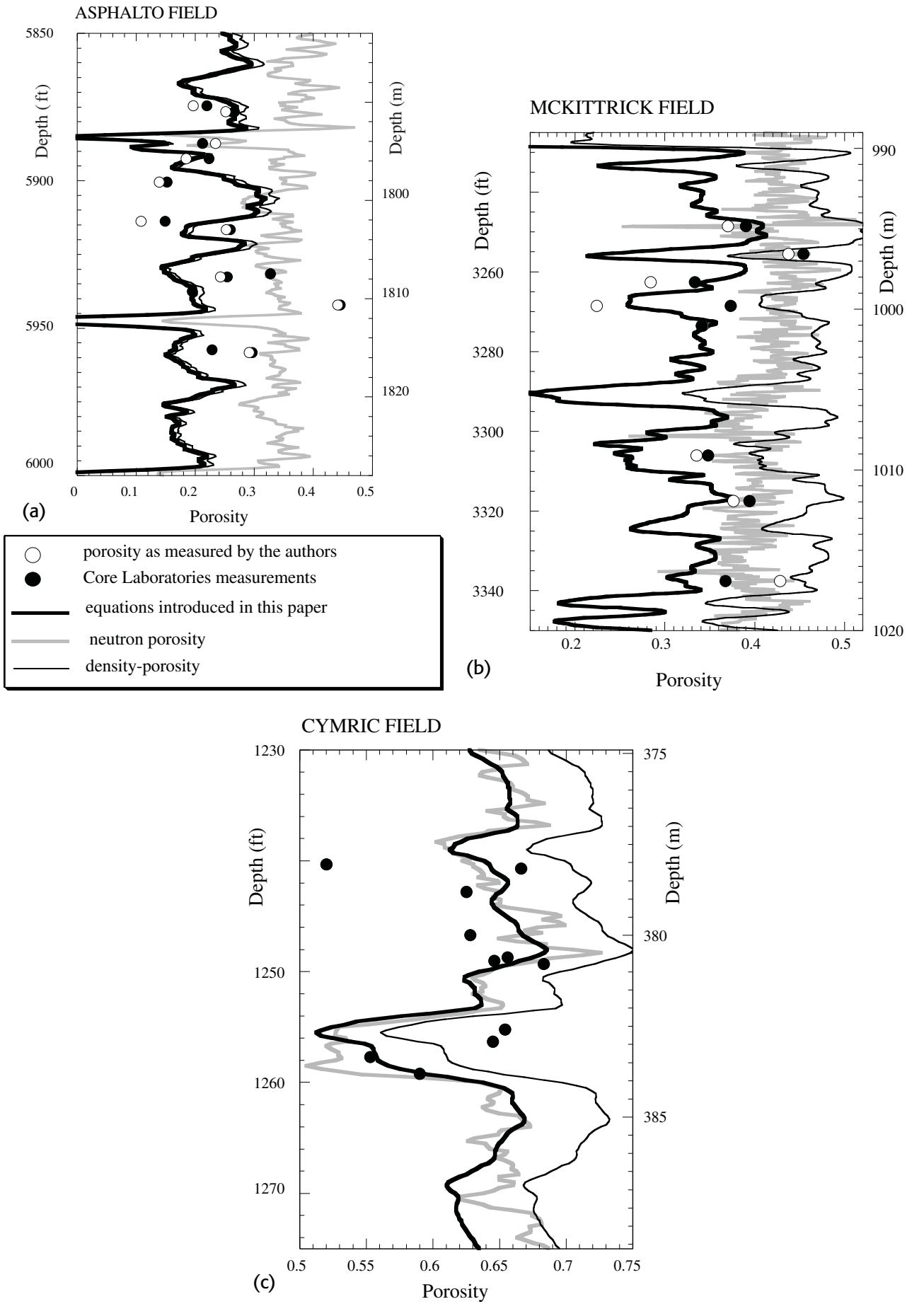
ASPHALTO FIELD
Depth (ft)
Depth (m)
5850
5900
5950
6000
1800
1810
1820
0
0.1
0.2
0.3
0.4
0.5
Porosity
(a)
porosity as measured by the authors
Core Laboratories measurements
equations introduced in this paper
neutron porosity
density-porosity
MCKITTRICK FIELD
Depth (ft)
Depth (m)
3260
3280
3300
3320
3340
990
1000
1010
1020
0.2
0.3
0.4
0.5
Porosity
(b)
CYMRIC FIELD
Depth (ft)
Depth (m)
1230
1250
1260
1270
375
380
385
0.5
0.55
0.6
0.65
0.7
0.75
Porosity
(c)

mineralogy occur gradually, and there is no abrupt diagenetic transition to create an acoustic reflector. Because these rocks follow a diagenetic pathway different from group 2 rocks, group 1 rocks retain matrix porosity to a greater burial depth and/or higher degree of diagenetic grade than do group 2 rocks. group 2 rocks are characterized by sharp diagenetic boundaries, accompanied by abrupt changes in porosity, density, and mineralogy. Matrix porosity is occluded in these rocks by silica overgrowths added during the crystal aging process, creating brittle, homogeneously textured rocks ideal for fracturing but having almost no matrix porosity. These rocks, which represent the stereotypical Monterey Formation fractured reservoir, are more likely to be characterized by an acoustic reflector at silica diagenetic boundaries.

We initially predicted that all San Joaquin basin rocks would plot as group 1 reservoirs and all coastal California rocks would plot as group 2. Because the San Joaquin is an inboard basin, its rocks have a higher clastic content and are therefore likely to follow the diagenetic pathway of impure rocks (Figure 6b). The coastal California outboard basins contain more purely siliceous rocks and should follow the pathway of Figure 6a to become fractured reservoirs.

The McKittrick field data from the San Joaquin basin, however, proved this generalization wrong. Whereas most of the inboard basin samples plot as group 1 and most of the outboard basin samples plot as group 2, the McKittrick field samples act as an important warning that there are exceptions to this rule. We recommend that investigators plot ρ_b/ϕ data from the logs of either their drilled prospect or a nearby analog well to determine which type of porosity system their prospective reservoir contains. The differences are important, as the drilling and completion fluids, hydraulic fracturing program, and other drilling, completion, and production plans should be very different for a relatively pure, fracture porosity–dominated group 2 reservoir than for a clay-rich group 1 reservoir that has fewer fractures but much more oil and gas storage in matrix porosity.

Preliminary results indicate our model can be used to classify biogenic siliceous reservoirs of the Monterey Formation as fracture-dominated or matrix porosity–dominated. To test this, we used dry bulk density and porosity data from a Monterey Formation reservoir known to be matrix porosity–dominated at Elk Hills field. The model correctly classified this reservoir as group 1.

Although the model was developed using dry bulk density, it can be resaturated and the regression lines flipped to allow porosity prediction from the saturated bulk density given on well logs. Use of this model permits more accurate porosity prediction, based on the density log, than is presently possible using standard estimation methods.

The Monterey Formation, with its wide areal extent, thick reservoirs, and rich oil reserves, represents one of the last frontiers of California oil and gas exploration. What we learn in successfully exploiting this resource can be applied around the Pacific Rim and in any other area containing diagenetically immature biogenic siliceous reservoir rocks.

APPENDIX: ANALYTICAL METHODS AND DATA TABULATION

Analytical Methods

We performed laboratory measurements on samples from five cores from San Joaquin Valley oil fields (Chaika, 1998): Shell (now Aera) well 565S1, from 1257 to 2493 ft (383–760 m) in North Belridge field (Sec. 1, T28S, R20E); Mobil (now Aera) well 8360A-2, from 1694 to 1976 ft (517–603 m) in South Belridge field (Sec. 2, T29S, R21E); Chevron well 1407R, from 1240 to 1260 ft (378–384 m) in Cymric field (Sec. 1, T30S, R21E); Chevron well 342–17Z, from 3248 to 3684 ft (991–1124 m) in McKittrick field (Sec. 17, T30S, R22E); and Chevron well 332X-25Z, from 5874 to 5958 ft (1792–1817 m) in Asphalto field (Sec. 25, T30S, R22E).

The samples had been dried by Core Laboratories Bakersfield (CLB) prior to our receiving them and were kept humidified throughout analysis. We weighed the samples then measured diameter and length to calculate volume. Porosity of samples were measured using a helium porosimeter. We determined dry bulk density by solving the equation

$$\text{dry bulk density } (\rho_{b(dry)}) = \text{total weight/total volume} \quad (14)$$

The CLB performed duplicate analyses on these samples and provided mineralogy data. According to Allen Britton, manager at CLB, (1996, personal communication), pore fluid extraction was done by the Dean Stark method. This involves cleaning samples using boiling toluene at approximately 115°C and removing the residue using methylene chloride, which boils at about 45°C. All samples were dried at approximately 115°C for between 4 and 48 hours. Rocks were weighed after all pore fluids were extracted, and then grain volume was determined using Boyle's law, using helium as the gaseous medium. Grain density was calculated using the equation

$$\text{grain density } (\rho_s) = \text{weight of solid/volume of solid} \quad (15)$$

Dry bulk density was calculated from porosity and grain density using the relationship

$$\rho_{b(dry)} = \rho_s(1 - \phi) \quad (16)$$

The CLB determined sample mineralogy using the semiquantitative Fourier transform infrared spectroscopy (FTIR) method, as per Harville and Freeman (1988) and Rice et al. (1995). The FTIR method, which is becoming increasingly popular in a wide variety of applications, measures infrared spectra radiated by minerals, as molecular bonds vibrate in response to application of infrared energy. Unlike x-ray diffraction (XRD), the FTIR method measures all frequencies at the same time, rather than moving sequentially through a range of wavelengths. The FTIR data collection is therefore easier and provides equally reliable qualitative to semiquantitative mineralogical identifications. Note that CLB directly measured ρ_s and ϕ and then calculated $\rho_{b(dry)}$, whereas we directly measured $\rho_{b(dry)}$ and ϕ and then calculated ρ_s. Agreement between the two data sets is remarkably good.

For graphical analysis, we assumed measured data are more accurate than calculated data. Therefore, we preferentially used our directly measured $\rho_{b(dry)}$ data and CLB's directly measured ρ_s data. No clear reason exists to prefer either CLB's ϕ data or our own. We chose to use the ϕ measurement that corresponds to the density measurement used in each case.

Our sources for coastal California Monterey Formation data are published information of Compton (1991) for Point Pedernales and Isaacs (1980) for the Santa Barbara area (Chaika, 1998). Both authors used XRD as the primary tool for measuring mineralogy. Like FTIR, this method is semiquantitative. It involves mounting a powdered sample on a slide, in such a way as to avoid preferred orientation of grains on the slide, and then subjecting it to alpha radiation from a copper source (CuKα radiation). Minerals having strong cleavage planes, however, tend to orient along these planes and create artificially strong peak intensities. Also, high iron or organic matter content in the sample interferes with CuKα radiation, causing background fluorescence that interferes with peak intensity (Bloss, 1971). Recognizing these limitations, both Isaacs (1980) and Compton (1991) made efforts to maximize quantitative accuracy through the use of supplemental analyses, such as elemental analysis, organic carbon analysis, x-ray fluorescence (XRF), thin-section petrography, and scanning electron microscopy (SEM). Indeed, Isaacs (1980) provides one of the most painstaking and rigorous attempts to reliably quantify mineralogy of fine-grained rocks in the geological literature.

Compton's (1991) and Isaacs's (1980) density and porosity data were collected in slightly different ways than those we have discussed for our data and that of CLB. For Compton (1991), cylindrical plugs were cut from rock samples, and bitumen was extracted using a chloroform-acetone solution. Petroleum Testing Service, Inc. (PTS) measured ϕ and ρ_s using Archimedes' principle. Plugs were dried overnight at 105°C and then weighed dry. They were then impregnated with toluene and immersed in a toluene bath and reweighed. Accuracy of porosity measurements was reported to be $\pm 0.5\%$ (Compton, 1991).

Although there are slight differences in methodology between our work and that of CLB and Compton (1991), the most significant methodological difference lies with Isaacs (1980). Porosity was calculated from direct ρ_s and $\rho_{b(dry)}$ measurements, made after heating samples at 100–105°C for 24 hours to remove bound water in clay and opaline grains. Samples were then kept in a dessicator to ensure that no rehydration occurred before density measurements were taken. All other studies for which density measurements are used in our present study were done on humidified samples—that is, samples that were allowed to equilibrate with the atmosphere after drying. As Isaacs herself points out, "Dry and humidified values of porosity may differ considerably—by 7 to 15 porosity % for opal-CT bearing rocks with 5 to 10% adsorbed water by weight—and are not easily compared" (Isaacs, 1981, p. 260).

Given the potential for 7–15% discrepancies in density/porosity values between Isaacs's (1980) dessicated samples and the humidified sample data of all other studies, we omit Isaacs (1980) data from our density/porosity discussion. An alternative would be to adjust dessicated porosities upward by some arbitrary value between 7 and 15% to rehumidify them. This would, however, introduce a large systematic error, and we chose not to do this. Therefore, we reserve Isaacs (1980) data for mineralogy-based discussions only.

Only rock samples having a silica content of at least 40 wt. % were used for this study. The 40 wt. % cutoff eliminated all high carbonate Point Pedernales samples from the Compton (1991) data set. We felt it was important to eliminate these data, because presence of high concentrations of either calcite or dolomite significantly complicates the diagenetic story (Isaacs, 1980) and is a stratigraphically localized rather than a general phenomenon. Besides high carbonate samples, this filtering process also eliminates clastic lithologies, such as sandstones, siltstones, and clay shales, that can be interbedded with rocks of biogenic origin.

If the sample contained opal-A, we assumed all sample quartz was detrital, because it is highly unlikely that there would be measurable diagenetic quartz in an opal-A dominated sample. If the sample contained opal-CT, we assumed the sample quartz was biogenic. As a control sample for the disordered opal-CT phase, we used density measurements performed on a zero-porosity, hydrothermal silica sample from Nevada, purchased from Wards catalog. The XRD analysis indicated that this sample was pure tridymite, a high temperature, moderate pressure polymorph of quartz (Deer et al., 1974). This is a reasonable standard to use, as the name opal-CT derives from the fact that this mineraloid is made up of interlayered stacks of cristobalite and tridymite domains.

Data Tabulation

In Table 2, "Other Rho(b)," "Other Rho(s)," and "Other Porosity" are the $\rho_{b(dry)}$, ρ_s, and ϕ data, respectively, that we received from CLB. "Our Rho(b)," "Our Rho(s)," and "Our Porosity" are the $\rho_{b(dry)}$, ρ_s, and ϕ data, respectively, that we collected. In $\rho_{b(dry)}/\phi$ regressions, we preferentially used our measured $\rho_{b(dry)}$ rather than those calculated by CLB. In such cases, we used the associated ϕ from the "Our Porosity" column. Where we did not measure $\rho_{b(dry)}$, we used "Other Rho(b)" data and the associated "Other Porosity." These selected data for graphical and statistical analysis of $\rho_{b(dry)}/\phi$ regression trends are listed again in the "Rho(b) for plotting" and "Por. to plot w/Rho(b)" columns. In the ρ_s analysis, we used CLB's measured ρ_s ("Other Rho(s)") exclusively and the associated porosities ("Other Porosity"). Missing data are represented by zeroes, as are nondetects. "Total biogenic silica" = opal-A + opal-CT + biogenic quartz. "Total nonsilica + clastics" = total clay + detrital quartz + other minerals. Depth is reported in feet, densities are reported in g/cm^3, and all mineralogical reports are by weight. Porosity measurements are by volume.

Table 2. Previously Unpublished Data Used in Regression Analysis*

Group	Field	Depth (ft)	Other Rho(b)	Our Rho(b)	Other Porosity	Our Porosity	Other Rho(s)	Our Rho(s)	Por. to plot w/Rho(b)	Rho(b) for Plotting	Opal-A (by wt.)	Opal-CT (by wt.)	Biogenic Quartz (by wt.)	Total Biogenic Silica	Total Clay (by wt.)	Detrital Quartz (by wt.)	Other Minerals (by wt.)	Total Nonsilica + Clastics
1	Cymric	1240.3	1.09	.00	.520	.000	2.27	.00	.520	1.090	.420	.00	.00	.420	.000	.00	.580	.580
1	Cymric	1240.7	.75	.00	.666	.000	2.25	.00	.666	.750	.530	.25	.00	.780	.110	.02	.110	.240
1	Cymric	1242.8	.89	.00	.625	.000	2.37	.00	.625	.890	.000	.74	.00	.740	.140	.00	.120	.260
1	Cymric	1246.7	.84	.00	.628	.000	2.26	.00	.628	.840	.250	.47	.00	.720	.180	.00	.100	.280
1	Cymric	1248.7	.80	.00	.656	.000	2.33	.00	.656	.800	.410	.36	.00	.770	.130	.00	.100	.230
1	Cymric	1249.0	.80	.00	.646	.000	2.26	.00	.646	.800	.720	.16	.00	.880	.080	.00	.040	.120
1	Cymric	1249.3	.70	.00	.683	.000	2.21	.00	.683	.700	.570	.28	.00	.850	.000	.00	.150	.150
1	Cymric	1255.2	.78	.00	.654	.000	2.25	.00	.654	.780	.000	.77	.00	.770	.150	.00	.080	.230
1	Cymric	1256.3	.80	.00	.645	.000	2.25	.00	.645	.800	.230	.49	.00	.720	.120	.00	.160	.280
1	Cymric	1257.7	1.01	.00	.553	.000	2.26	.00	.553	1.010	.000	.78	.00	.780	.150	.00	.070	.220
1	Cymric	1259.2	.94	.00	.590	.000	2.29	.00	.590	.940	.000	.64	.00	.640	.220	.00	.140	.360
1	Asphalto	5874.5	1.99	1.85	.219	.196	2.55	2.30	.196	1.850	.000	.00	.55	.548	.220	.00	.182	.402
1	Asphalto	5876.5	1.86	1.90	.266	.251	2.53	2.54	.251	1.900	.000	.00	.70	.700	.130	.00	.170	.300
1	Asphalto	5887.3	1.97	1.91	.212	.234	2.50	2.49	.234	1.910	.000	.00	.65	.650	.180	.00	.170	.350
1	Asphalto	5892.5	1.96	2.00	.223	.184	2.52	2.45	.184	2.000	.000	.00	.67	.670	.180	.00	.150	.330
1	Asphalto	5900.4	2.15	2.12	.152	.139	2.54	2.46	.139	2.120	.000	.00	.46	.460	.310	.00	.230	.540
1	Asphalto	5913.7	2.16	2.16	.149	.108	2.54	2.42	.108	2.160	.000	.00	.42	.423	.296	.00	.246	.542
1	Asphalto	5916.5	1.88	1.88	.259	.252	2.54	2.51	.252	1.880	.000	.00	.67	.670	.170	.00	.160	.330
1	Asphalto	5931.5	1.72	.00	.327	.000	2.56	.00	.327	1.720	.000	.15	.57	.716	.115	.00	.140	.255
1	Asphalto	5932.5	1.90	1.88	.254	.242	2.55	2.48	.242	1.880	.000	.19	.55	.731	.097	.00	.140	.237
1	Asphalto	5937.5	1.96	.00	.195	.000	2.43	.00	.195	1.960	.000	.46	.36	.826	.060	.00	.090	.150
1	Asphalto	5942.1	1.42	1.40	.445	.441	2.56	2.50	.441	1.400	.000	.31	.45	.756	.132	.00	.086	.218
1	Asphalto	5957.3	1.96	.00	.228	.000	2.54	.00	.228	1.960	.000	.00	.66	.664	.136	.00	.166	.302
1	Asphalto	5958.2	1.82	1.78	.296	.291	2.59	2.51	.291	1.780	.000	.32	.44	.761	.106	.00	.116	.222
1	S Belridge	1694.0	.98	.00	.577	.000	2.32	.00	.577	.981	.440	.00	.00	.440	.280	.08	.200	.560

1	S Belridge	1714.0	1.00	.00	.572	.000	2.34	.00	.572	1.001	.420	.00	.00	.420	.290	.10	.190	.580
1	S Belridge	1846.0	1.15	.00	.522	.000	2.40	.00	.522	1.147	.400	.00	.00	.400	.310	.08	.210	.600
1	S Belridge	1882.0	.89	.00	.606	.000	2.27	.00	.606	.894	.360	.21	.00	.570	.250	.00	.180	.430
1	S Belridge	1895.0	.99	.00	.570	.000	2.30	.00	.570	.989	.270	.25	.00	.520	.260	.02	.200	.480
1	S Belridge	1906.0	1.29	.00	.443	.000	2.31	.00	.443	1.287	.000	.41	.00	.410	.360	.04	.190	.590
1	S Belridge	1930.0	1.44	.00	.411	.000	2.45	.00	.411	1.443	.190	.23	.00	.420	.340	.00	.240	.580
1	N Belridge	1257.0	.92	.00	.614	.000	2.39	.00	.614	.922	.530	.00	.00	.530	.240	.05	.300	.590
1	N Belridge	1745.0	.92	.00	.615	.000	2.38	.00	.615	.916	.490	.00	.00	.490	.260	.09	.250	.600
1	N Belridge	1761.0	.87	.00	.634	.000	2.38	.00	.634	.871	.570	.00	.00	.570	.150	.08	.180	.410
1	N Belridge	1796.0	1.09	.00	.552	.000	2.44	.00	.552	1.093	.420	.00	.00	.420	.260	.12	.160	.540
1	N Belridge	1920.0	.73	.00	.686	.000	2.31	.00	.686	.725	.660	.00	.00	.660	.150	.06	.120	.330
1	N Belridge	1975.0	1.12	.00	.535	.000	2.40	.00	.535	1.116	.330	.21	.00	.540	.230	.07	.130	.430
1	N Belridge	2010.0	1.05	.00	.567	.000	2.42	.00	.567	1.048	.000	.61	.00	.610	.180	.02	.120	.320
1	N Belridge	2107.0	1.24	.00	.495	.000	2.46	.00	.495	1.242	.000	.47	.00	.470	.260	.00	.250	.510
2	McKittrick	3248.5	1.38	1.39	.390	.370	2.26	2.21	.370	1.390	.000	.67	.00	.670	.090	.00	.240	.330
2	McKittrick	3255.5	1.20	1.22	.454	.437	2.20	2.17	.437	1.220	.000	.88	.00	.880	.000	.00	.120	.120
2	McKittrick	3262.5	1.45	1.42	.333	.284	2.17	1.98	.284	1.420	.000	.97	.00	.970	.030	.00	.000	.030
2	McKittrick	3268.5	1.47	1.49	.373	.224	2.34	1.92	.224	1.490	.000	.95	.00	.950	.000	.00	.050	.050
2	McKittrick	3273.5	1.47	1.42	.341	.342	2.23	2.16	.342	1.420	.000	.71	.00	.710	.100	.00	.190	.290
2	McKittrick	3306.0	1.46	1.48	.348	.335	2.24	2.23	.335	1.480	.000	.71	.00	.710	.120	.00	.170	.290
2	McKittrick	3317.5	1.35	1.36	.394	.376	2.23	2.18	.376	1.360	.000	.86	.00	.860	.140	.00	.000	.140
2	McKittrick	3337.5	1.38	1.23	.367	.428	2.18	2.15	.428	1.230	.000	.95	.00	.950	.050	.00	.000	.050
2	McKittrick	3600.5	1.33	1.32	.416	.394	2.28	2.18	.394	1.320	.000	.75	.00	.750	.120	.00	.130	.250
2	McKittrick	3603.5	1.27	1.29	.433	.412	2.24	2.19	.412	1.290	.000	.90	.00	.900	.060	.00	.040	.100
2	McKittrick	3606.5	1.31	1.25	.416	.441	2.24	2.24	.441	1.250	.000	.90	.00	.900	.100	.00	.000	.100
2	McKittrick	3670.5	1.49	1.52	.337	.290	2.25	2.14	.290	1.520	.000	.83	.00	.830	.120	.00	.050	.170
2	McKittrick	3678.5	1.48	1.45	.358	.360	2.31	2.27	.360	1.450	.000	.67	.00	.670	.170	.00	.160	.330
2	McKittrick	3681.0	1.51	1.48	.343	.360	2.30	2.31	.360	1.480	.000	.65	.00	.650	.230	.00	.120	.350
2	McKittrick	3684.5	1.33	1.27	.418	.421	2.29	2.19	.421	1.270	.000	.87	.00	.870	.130	.00	.000	.130

** Santa Barbara data, Point Pedernales data, and Elk Hills data used in this study can be found in Isaacs (1980), Compton (1991), and Reid and McIntrye (2001), respectively.*

REFERENCES CITED

Badaut, D., and F. Risacher, 1983, Authigenic smectite on diatom frustules in Bolivian saline lakes: Geochimica, Cosmochimica Acta, v. 47, p. 363–375.

Blake, G. H., 1981, Biostratigraphy and correlation: problems in marginal basin development, San Joaquin Valley, California, *in* R. E. Garrison and R. G. Douglas, eds., The Monterey Formation and related siliceous rocks of California: Pacific Section SEPM Symposium Volume, book 15, p. 1–14.

Bloss, F. D., 1971, Crystallography and crystal chemistry: New York, Holt, Rhinehart and Winston, 544 p.

Bohrmann, G., V. Spiess, H. Hinze, and G. Kuhn, 1992, Reflector "Pc", a prominent feature in the Maud Rise sediment sequence (eastern Weddell Sea): occurrence, regional distribution and implications to silica diagenesis: Marine Geology, v. 106, p. 69–87.

Bramlette, M. N., 1946, The Monterey Formation of California and the origin of its siliceous rocks: U.S. Geological Survey Professional Paper 212, 57 p.

California Department of Conservation (CDOC) Division of Oil, Gas and Geothermal Resources, 1998, 1997 Annual report of the state oil and gas supervisor: Publication #PR06 267 p.

Chaika, C., 1998, Physical properties and silica diagenesis: Ph.D. dissertation, Stanford University, Stanford, California, 117 p.

Chang, J., and Y. C. Yortsos, 1994, Lamination during silica diagenesis—effects of clay content and Ostwald ripening: American Journal of Science, v. 294, p. 137–172.

Compton, J. S., 1991, Porosity reduction and burial history of siliceous rocks from the Monterey and Sisquoc formations, Point Pedernales, California: Geological Society of America Bulletin, v. 103, p. 625–636.

Cook, S. D., 1994, Advanced reservoir characterization in the Antelope Shale to establish the viability of CO_2 enhanced oil recovery in California's Monterey Formation siliceous shale: Project proposal to the Department of Energy, DOE #DE-PS22–94BC14973.

Deer, W. A., R. A. Howie, and J. Zussman, 1974, An introduction to the rock forming minerals, 7th ed.: London, Longman, 528 p.

Graham, S. A., and L. A. Williams, 1985, Tectonic, depositional and diagenetic history of Monterey Formation (Miocene), central San Joaquin basin, California: AAPG Bulletin, v. 69, p. 385–411.

Grivetti, M. C., 1982, Aspects of stratigraphy, diagenesis and deformation in the Monterey Formation near Santa Maria-Lompoc, California: Master's thesis, University of California at Santa Barbara, 155 p.

Gross, M. R., 1995, Fracture partitioning: failure mode as a function of lithology in the Monterey Formation of coastal California: Geological Society of America Bulletin, v. 107, no. 7, p. 779–792.

Harville, D. G., and D. L. Freeman, 1988, The benefits of application of rapid mineral analysis provided by Fourier transform infrared spectroscopy (abs.): Society of Petroleum Engineers 63rd Annual Technical Conference and Exhibition Proceedings, abstract 18120, p. 141–146.

Hein, J. R., D. W. Scholl, J. A. Barron, M. G. Jones, and J. Miller, 1978, Diagenesis of late Cenozoic diatomaceous deposits and formation of the bottom simulating reflector in the South Bering Sea: Sedimentology, v. 25, p. 155–181.

Hurd, D. C., 1983, Physical and chemical properties of siliceous skeletons, *in* S. Aston, ed., Silicon geochemistry and biogeochemistry: New York, Academic Press, p. 187–243.

Iijima, A., and R. Tada, 1981, Silica diagenesis of Neogene diatomaceous and volcaniclastic sediments in northern Japan: Sedimentology, v. 28, p. 185–200.

Iler, R. K., 1973, Colloidal silica, *in* E. Matijevic, ed., Surface and colloid science, v. 6: New York, Wiley, p. 1–100.

Iler, R. K., 1979, Chemistry of silica: New York, Wiley-Interscience, 866 p.

Ingle, J. C., 1981, Origin of Neogene diatomites around the North Pacific Rim, *in* R. E. Garrison and R. G. Douglas, eds., The Monterey Formation and related siliceous rocks of California: Pacific Section SEPM Symposium Volume, book 15, p. 159–180.

Isaacs, C. M., 1980, Diagenesis in the Monterey Formation examined laterally along the coast near Santa Barbara, California: Ph.D. dissertation, Stanford University, Stanford, California, 329 p.

Isaacs, C. M., 1981, Porosity reduction during diagenesis of the Monterey Formation, Santa Barbara coastal area, California, *in* R. E. Garrison and R. G. Douglas, eds., The Monterey Formation and related siliceous rocks of California: Pacific Section SEPM Symposium Volume, book 15, p. 257–272.

Isaacs, C. M., 1983, Compositional variation and sequence in the Miocene Monterey Formation, Santa Barbara coastal area, California, *in* D. K. LaRue and R. J. Steel, eds., Cenozoic marine sedimentation, Pacific margin, USA: Pacific Section SEPM Publication, p. 117–132.

Kästner, M., J. B. Keene, and J. M. Gieskes, 1977, Diagenesis of siliceous oozes, I: chemical controls on the rate of opal-A to opal-CT transformation—an experimental study: Geochimica, Cosmochimica Acta, v. 41, p. 1041–1059.

Lonsdale, M. J., 1990, The relationship between silica diagenesis, methane, and seismic reflections on the South Orkney microcontinent, *in* P. F. Barker et al., eds., 1990 Proceedings of the ocean drilling program, scientific results: v. 113, p. 27–37.

Luyendyk, B. P., and J. S. Hornafius, 1987, Neogene crustal rotation, fault slip and basin development in Southern California, *in* R. V. Ingersoll and W. G. Ernst, eds., Rubey volume VI: Cenozoic basin development of coastal California: Englewood Cliffs, New Jersey, Prentice-Hall, p. 259–283.

Mayerson, D. A., and J. Crouch, 1994, The opal-CT/quartz diagenetic boundary within the Monterey Formation of the California offshore Santa Maria Basin; an untapped exploration target (abs.): AAPG Bulletin, v. 78, no. 4, p. 669–670.

Mayerson, D. A., C. A. Dunkel, K. A. Piper, and H. L. Cousminer, 1995, Identification and correlation of the opal-CT/quartz phase transition in offshore central California (abs.): AAPG Bulletin, v. 79, no. 4, p. 592.

McGill, G. E., and J. A. Raney, 1970, Experimental study of faulting in an anisotropic inhomogeneous dolomitic limestone: Geological Society of America Bulletin, v. 81, p. 2949–2958.

McManus, D. A., R. E. Burns, O. Weser, T. Vallier, C. V. von der Borch, R. K. Olsson, R. M. Goll, and E. D. Milow, 1970, Initial reports of the deep sea drilling project, volume V: Washington, D.C., U.S. Government Printing Office, 827 p.

Murata, K. J., and R. R. Larsen, 1975, Diagenesis of Monterey siliceous shales, Temblor Range, California: United States Geological Survey Journal of Research, v. 3, p. 553–566.

Oehler, J. H., 1975, Origin and distribution of silica lepispheres in porcelanite from the Monterey Formation of California: Journal of Sedimentary Petrology, v. 45, p. 252–257.

Pisciotto, K. A., and R. E. Garrison, 1981, Lithofacies and depositional environments of the Monterey Formation, California, *in* R. E. Garrison and R. G. Douglas, eds., The Monterey Formation and related siliceous rocks of California: Pacific Section SEPM Symposium Volume, book 15, p. 97–122.

Reid, S. A., and J. L. McIntyre, 2001, Monterey Formation porcelanite reservoirs of the Elk Hills field, Kern County, California: AAPG Bulletin, v. 85, no. 1, p. 169–189.

Rice, S. B., H. Freund, W.-L. Huang, J. A. Clouse, and C. M. Isaacs, 1995, Application of Fourier transform infrared spectroscopy to silica diagenesis: the opal-A to opal-CT transformation: Journal of Sedimentary Research, v. A65, no. 4, p. 639–647.

Schlumberger, 1989, Log interpretation principles/applications: Houston, Schlumberger Education Services, not paginated.

Schoell, M., S. Schouten, J. S. Sinninghe Damsté, J. W. De Leeuw, and R. E. Summons, 1994, A molecular carbon isotope record of Miocene climate changes: Science, v. 263, p. 1122–1125.

Shipley, T. H., M. H. Houston, R. T. Buffler, F. J. Shaub, K. J. McMillen, J. W. Ladd, and J. L. Worzel, 1979, Seismic evidence for widespread possible gas hydrate horizons on continental slopes and rises: AAPG Bulletin, v. 63, no. 12, p. 2204–2213.

Snyder, W. S., H. K. Brueckner, and R. A. Schweikert, 1983, Deformational styles in the Monterey Formation and other siliceous sedimentary rocks, *in* C. M. Isaacs and R. E. Garrison, eds., Petroleum generation and occurrence in the Miocene Monterey Formation, California: Pacific Section SEPM Volume, p. 151–170.

Tada, R., and A. Iijima, 1983, Petrology and diagenetic changes of Neogene siliceous rocks in northern Japan: Journal of Sedimentary Petrology, v. 53, no. 3, p. 911–930.

Williams, L. A., 1982, Lithology of the Monterey Formation (Miocene) in the San Joaquin Valley of California, *in* L. A. Williams and S. A. Graham, eds., Monterey Formation and associated coarse clastic rocks, central San Joaquin basin, California: Pacific Section SEPM Publication 25, p. 17–36.

Williams, L. A., 1988, Origins of reservoir complexity in the Miocene Monterey Formation of California, *in* S. A. Graham, ed., Studies of the geology of the San Joaquin basin: Pacific Section SEPM, v. 60, p. 261–279.

Williams, L. A., and D. A. Crerar, 1985, Silica diagenesis II: general mechanisms: Journal of Sedimentary Petrology, v. 55, p. 312–321.

Williams, L. A., G. A. Parks, and D. A. Crerar, 1985, Silica diagenesis I: solubility controls: Journal of Sedimentary Petrology, v. 55, p. 301–311.

Wise, S. W., and F. M. Weaver, 1974, Chertification of oceanic sediments, *in* K. J. Hsü and H. C. Jenkyns, eds., Pelagic sediments: on land and under the sea: International Association of Sedimentologists Special Publication 1, p. 301–326.